Applied Catalysis B: Environmental 236 (2018) 240–252

Contents lists available at ScienceDirect

Applied Catalysis B: Environmental

journal homepage: www.elsevier.com/locate/apcatb

The inhibition of hydrogen and oxygen recombination reaction by halogen atoms on over-all water splitting over Pt-TiO_2 photocatalyst

Meng Wang[a,b,c], Wenlong Zhen[a], Bin Tian[a,b], Jiantai Ma[c], Gongxuan Lu[a,*]

[a] State key Laboratory for Oxo Synthesis and Selective Oxidation, Lanzhou Institute of Chemical Physics, Chinese Academy of Science, Lanzhou, 730000, China
[b] University of Chinese Academy of Science, Beijing, 100049, China
[c] College of Chemistry and Chemical Engineering, Lanzhou University, Lanzhou, 730000, China

ARTICLE INFO

Keywords:
Halogen atoms
Inhibition of H_2 and O_2 recombination
Overall water splitting
Photocatalyst

ABSTRACT

Semiconductor photocatalysts for overall water splitting into H_2 and O_2 require metal cocatalyst, such as Pt, to catalyze H_2 evolution efficiently. However, these metal cocatalysts can also catalyze hydrogen and oxygen recombination to form water. In this paper, we found that the pre-adsorbed halogen atom catalyst could inhibit the reverse reaction of water formation from H_2 and O_2 due to the decrease of adsorption energies of H_2 and O_2 on Pt. The adsorption energy decrease of H_2 and O_2 followed the order of F/Pt < Cl/Pt < I/Pt < Br/Pt. H_2-TPD results exhibited similar dependence. This inhibition was achieved *via* the occupation of halogen atom on the Pt surface sites, and thereby the adsorption and activation of hydrogen and oxygen molecules were decreased. The occupation difference of halogen atoms are determined by radius of halogen ions, which further leads the different activity for H_2 and O_2 recombination. By inhibition of water formation reverse reaction, the over-all water splitting over various TiO_2 photocatalysts has been achieved. Isotope experiments with D_2O and $H_2{}^{18}O$ confirmed the over-all water splitting to H_2 and O_2. This study may help scientist to develop high-efficient photocatalyst for overall water splitting.

1. Introduction

To effectively address the problems related to the fast depletion of fossil fuels and the increasing environmental pollution, the development of renewable energy, especially conversion and storage of solar energy has attracted extensive attentions recently [1–23]. Hydrogen is considered as one of the most ideal energy carrier in the transfer of solar irradiation to clean chemical power source because of its zero-emission characteristics during its usage [24–38]. Many efforts have devoted to the production of hydrogen, including methane reforming [39–41], natural gas pyrolysis [42], water gas shift reaction (WGS) [43], biomass catalytic steam reforming/gasification [44], water splitting [45,46]. Among them, water splitting to hydrogen driven by sun light is a promising route *via* solar-thermal-pyrolytic water, photovoltaic plus electrolysis of water, and photocatalytic water splitting [47–49]. To achieve overall water splitting [50], low overpotential co-catalyst for hydrogen evolution reaction (HER) is necessary, such as noble metals Pt, Ru and Rh [51–55]. However, the Pt or other noble metal cocatalysts can also catalyze the hydrogen and oxygen recombination reaction back to water, remarkably reduced the efficiency of photocatalytic water splitting [45]. Therefore, it is of great importance to find the strategy to inhibit the hydrogen and oxygen recombination reaction while catalyze water splitting efficiently.

Many efforts have been made to suppress the H_2 and O_2 recombination reaction in overall water splitting. For instance, higher oxidation state Pt in PtO/TiO_2 photocatalyst can act as efficient hydrogen evolution site while suppress the undesirable hydrogen and oxygen recombination reaction [56]. GaN nanowires with Rh/Cr_2O_3 core-shell nanostructure cocatalyst can prevent water forming back reaction by the O_2 diffusion barrier of Cr_2O_3 shell [30]. Interestingly, pre-chemisorbed CO on metal co-catalysts (Rh, Pt, Pd) can also suppress the H_2 and O_2 recombination back reaction while maintain the rate of H_2 evolution [57]. Adding small amount of iodine ion into the aqueous suspension of Pt-TiO_2 catalyst can preferentially adsorb onto Pt co-catalyst as well, and this iodine layer can effectively suppress the backward reaction of water formation from H_2 and O_2 over the Pt surface [58,59].

H_2 and O_2 recombination reaction over noble metal co-catalysts was due to their activation property for H_2 and O_2, over which H_2 and O_2 molecule can dissociate into atomic H and atomic O to form water. Fortunately, halogen atom would prefer adsorb on the catalyst surface, forming relatively strong interaction with the surface metal atoms due

* Corresponding author.
E-mail address: gxlu@lzb.ac.cn (G. Lu).

https://doi.org/10.1016/j.apcatb.2018.05.031
Received 5 February 2018; Received in revised form 17 April 2018; Accepted 9 May 2018
Available online 10 May 2018
0926-3373/ © 2018 Elsevier B.V. All rights reserved.

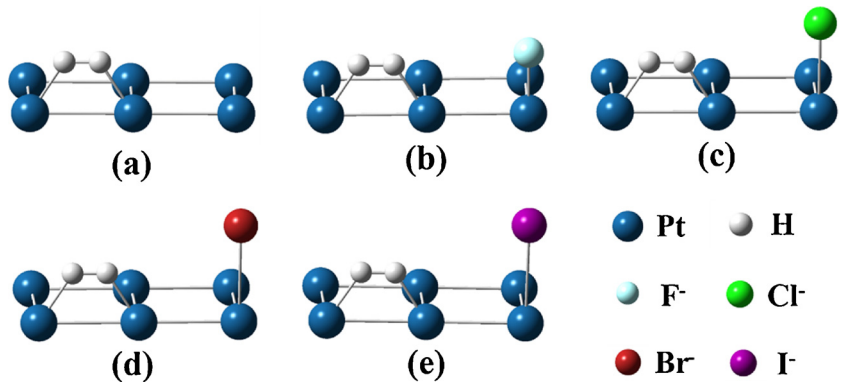

Fig. 1. Hydrogen molecule adsorbed on $Pt_6(100)$ surface: (a) Pt, (b) F/Pt, (c) Cl/Pt, (d) Br/Pt, (e) I/Pt.

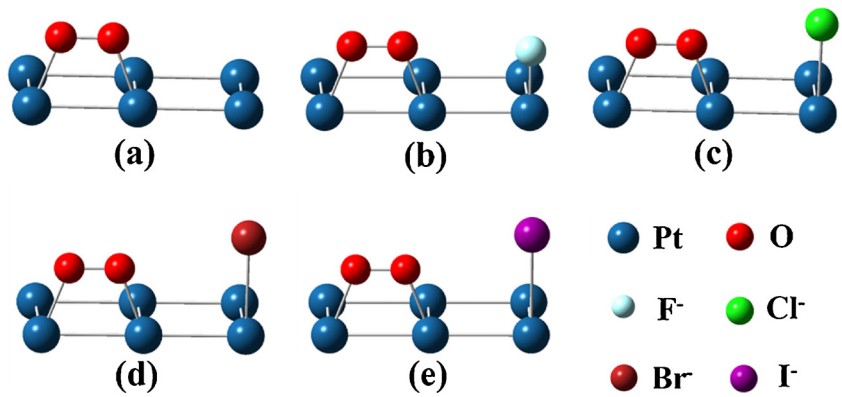

Fig. 2. Oxygen molecule adsorbed on $Pt_6(100)$ surface: (a) Pt, (b) F/Pt, (c) Cl/Pt, (d) Br/Pt, (e) I/Pt.

Table 1
H_2 and O_2 molecule adsorbed on pristine Pt and halogen ion pre-adsorbed Pt surface.

Catalysts	Adsorption energy (eV)	
	H_2	O_2
Pt	−0.92	−1.67
F/Pt	−0.22	−1.21
Cl/Pt	−0.47	−1.38
Br/Pt	−0.52	−1.43
I/Pt	−0.49	−1.39

Table 2
H_2 and O_2 molecule adsorbed on pristine Pt and fluorine ion adsorbed Pt surface.

Catalysts	Adsorption energy (eV)	
	H_2	O_2
Pt	−1.14	−1.89
F/Pt 1	−0.65	−1.59
F/Pt 2	−0.77	−1.77
F/Pt 1, F/Pt 2	−0.32	−1.45

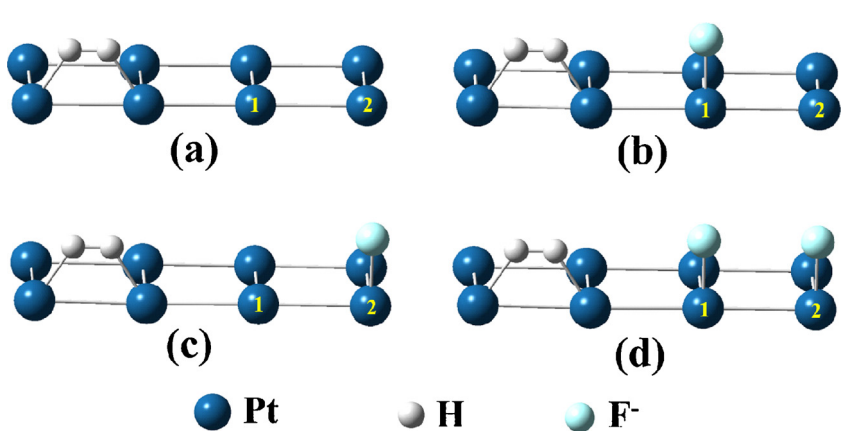

Fig. 3. Hydrogen molecule adsorbed on clean $Pt_8(100)$ surface (a) and fluorine ion modified $Pt_8(100)$ surface.

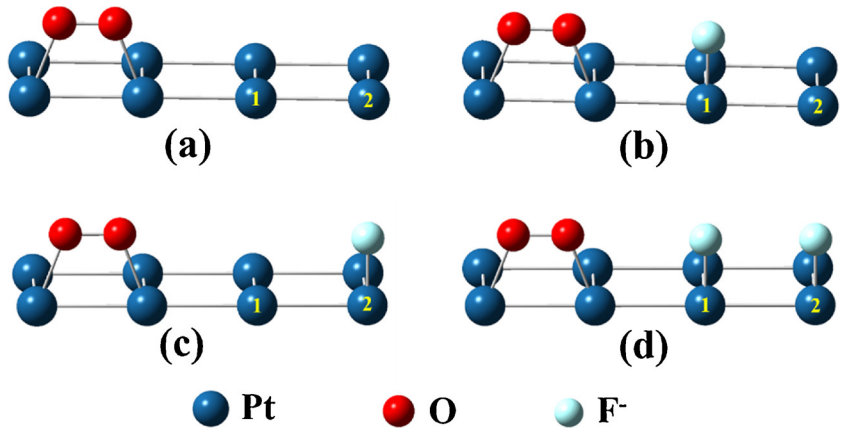

Fig. 4. Oxygen molecule adsorbed on clean $Pt_8(100)$ surface (a) and fluorine ion adsorbed $Pt_8(100)$ surface (b–d).

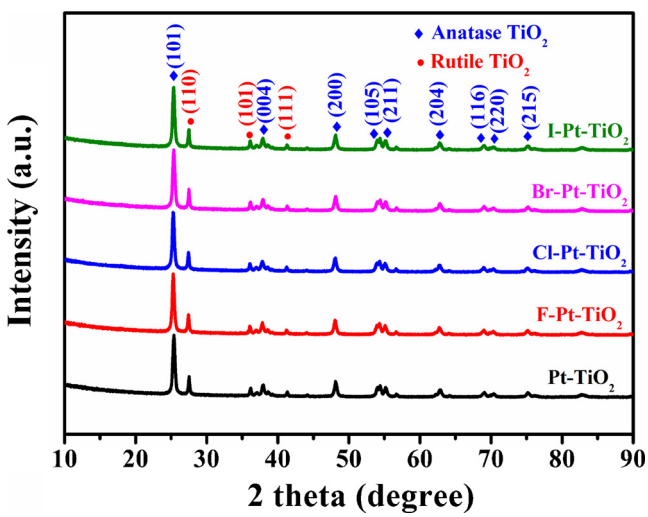

Fig. 5. XRD patterns of Pt-TiO_2, F-Pt-TiO_2, Cl-Pt-TiO_2, Br-Pt-TiO_2, and I-Pt-TiO_2 catalysts.

to the strong electronegativity of halogen atoms [60]. Therefore, catalyst with pre-adsorbed halogen atom can suppress the water forming reverse reaction by hindering the adsorption and activation of H_2 and O_2 molecules. In order to recover the mechanism of inhibition role of different halogen atoms, the effects of halogen element electronegativity, adsorption type and spatial occupation on both hydrogen farming forward reaction and water forming reverse reaction should be investigated before synthesizing effective catalyst for over-all water splitting. In this paper, we systemically compared the halogen ions adsorbed Pt-TiO_2 catalysts (F-Pt-TiO_2, Cl-Pt-TiO_2, Br-Pt-TiO_2, I-Pt-TiO_2) on the inhibition of H_2 and O_2 recombination reaction. By detail theoretical and experimental analysis, the inhibition mechanism of different halogen atoms was illustrated. We found that the presence of trace amount of halogen ions could inhibit the H_2 and O_2 recombination significantly by decreasing the hydrogen and oxygen molecule adsorption. The over-all water splitting driven by light was achieved by inhibition of H_2 and O_2 recombination over halogen ions. The difference of halogen element inhibition ability on H_2 and O_2 recombination was induced by their different spatial occupation on Pt surface. These results will help scientist to develop new highly efficient catalyst for over-all water splitting.

2. Experimental

2.1. Materials

All chemicals were commercial purchased and used without further purification. Commercial powder P25 TiO_2 (Deguss Corp.), chloroplatinic acid, ($H_2PtCl_6{\cdot}6H_2O$, Tianjin Kemiou Chemical Reagent Co., Ltd, AR, ≥99.0%), ammonium fluoride (NH_4F, Tianjin Kemiou Chemical Reagent Co., Ltd, AR, ≥99.0%), ammonium chloride (NH_4Cl, Xilong Chemical Co., Ltd., AR, > 99%), ammonium bromide (NH_4Br, Tianjin Fengyue Chemical Reagent Co., Ltd, AR, ≥99.0%), ammonium iodide (NH_4I, Shanghai Saen Chemical Reagent Co., Ltd, AR, > 99%).

2.2. Catalysts preparation

Pt-TiO_2 sample was synthesized by an impregnation and H_2 reduction method. 1 g of TiO_2 was added into a crucible containing 5.366 mL of chloroplatinic acid solution (9.654 mmol·L^{-1}) under magnetic stirring. After 2–3 h, the suspension was evaporated by an infrared lamp. Then, the resulting powders were calcined at 120 °C for 3 h and 400 °C for 5 h. After that, the catalyst was reduced under H_2 atmosphere at 300 °C for 3 h.

The adsorption of halogen ions on Pt-TiO_2 were achieved as follows: take F-Pt-TiO_2 as an example, 0.2 g of the as-prepared Pt-TiO_2 was dispersed in 150 mL appropriate concentration of NH_4F solution under vigorous stirring for two hours. The precipitates were then filtrated and washed with distilled water. After drying at room temperature, the obtained sample was labeled as F-Pt-TiO_2. The Cl-Pt-TiO_2, Br-Pt-TiO_2 and I-Pt-TiO_2 samples were obtained through the same treatment of Pt-TiO_2 by introducing the corresponding NH_4Cl, NH_4Br and NH_4I solutions, respectively.

2.3. Catalytic experiments

2.3.1. H_2 and O_2 recombination test

The H_2 and O_2 recombination test was performed in a sealed Pyrex flask (200 mL) with a flat window and a silicone rubber septum for sampling. Fifty milligrams of catalyst was added into pure water (150 mL), then was treated with ultrasound to make it dispersed well. The air in the system was evacuated by bubbling Ar gas for 30 min. 1 mL H_2 and 1 mL O_2 was then injected into the reactor to conduct the H_2 and O_2 recombination experiment. The amount of H_2 and O_2 was detected by gas chromatography (Agilent 6820, TCD, 13 × column, Ar carrier).

2.3.2. Photocatalytic H_2 evolution test

The photocatalytic H_2 evolution test was carried out in the similar sealed Pyrex flask and irradiation under the UV light. The flask with

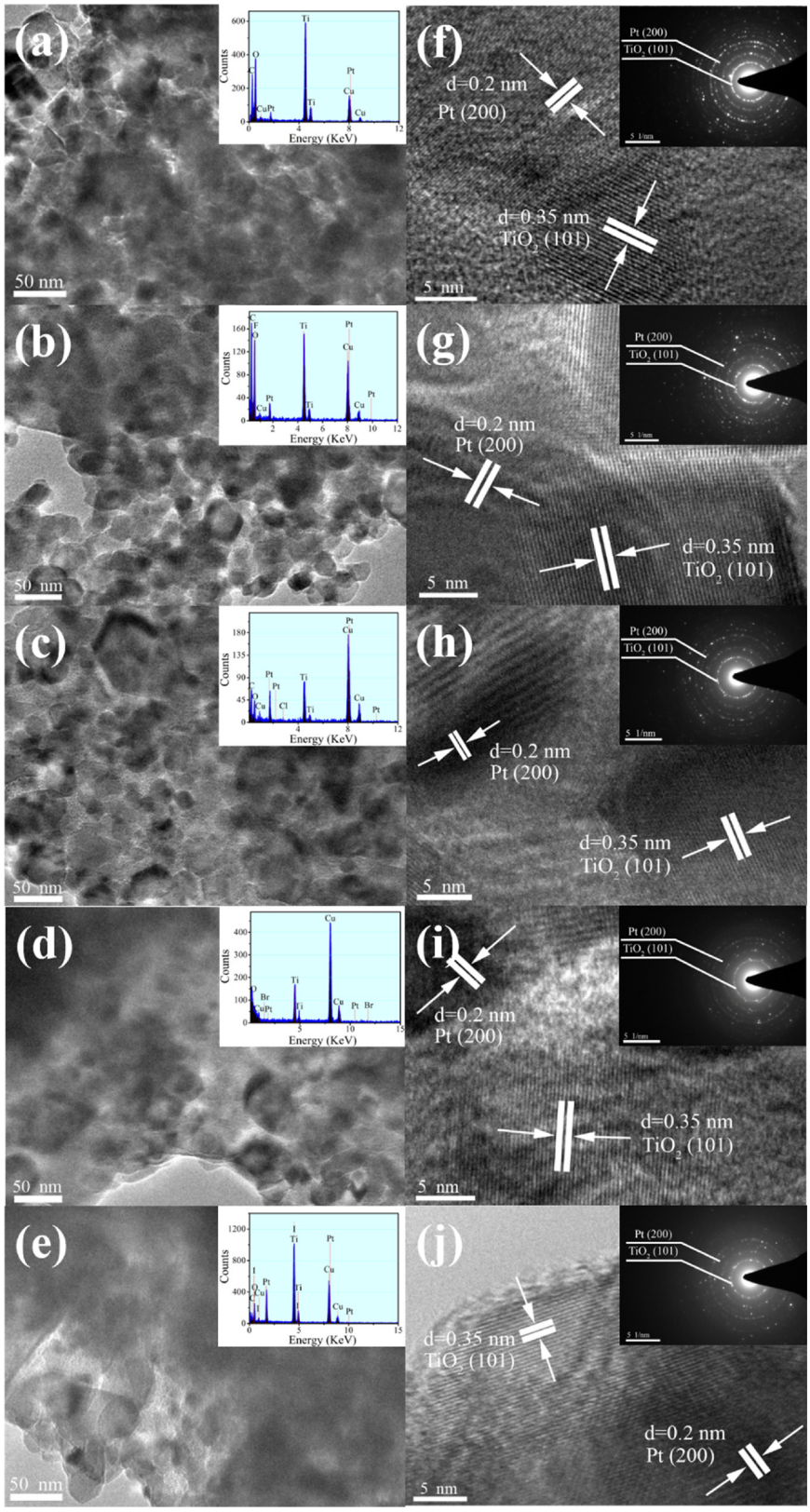

Fig. 6. TEM and HRTEM images of Pt-TiO_2 (a, f), F-Pt-TiO_2 (b, g), Cl-Pt-TiO_2 (c, h), Br-Pt-TiO_2 (d, i) and I-Pt-TiO_2 (e, j). (Inset shown the corresponding EDS spectra and SAED patterns).

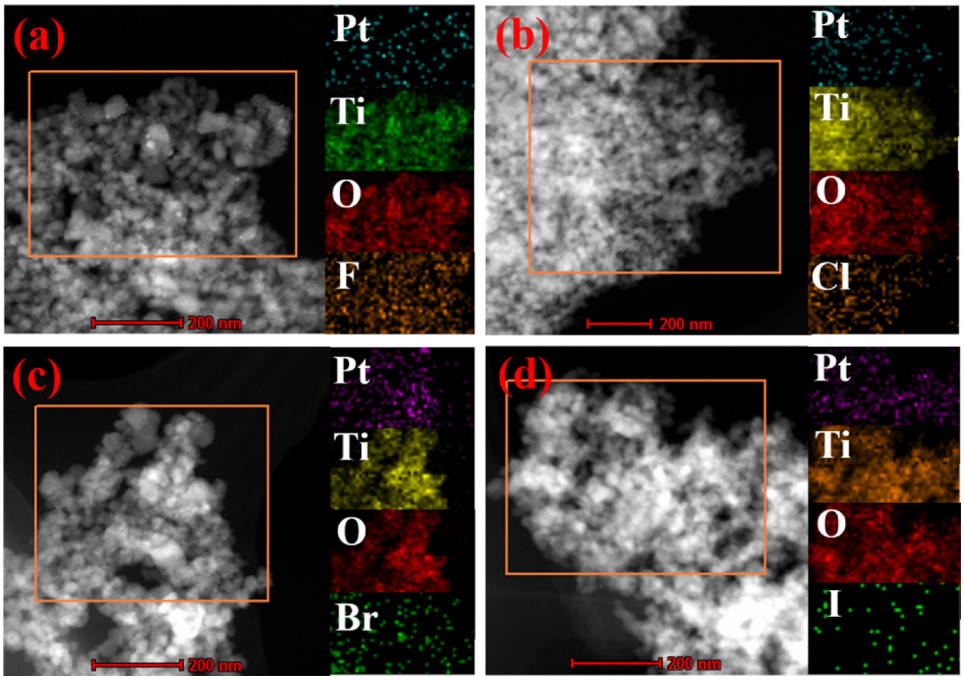

Fig. 7. HAADF-STEM (high-angle annular dark field scanning transmission electron microscopy) images and elemental mapping images of F-Pt-TiO_2 (a), Cl-Pt-TiO_2 (b), Br-Pt-TiO_2 (c), I-Pt-TiO_2 (d).

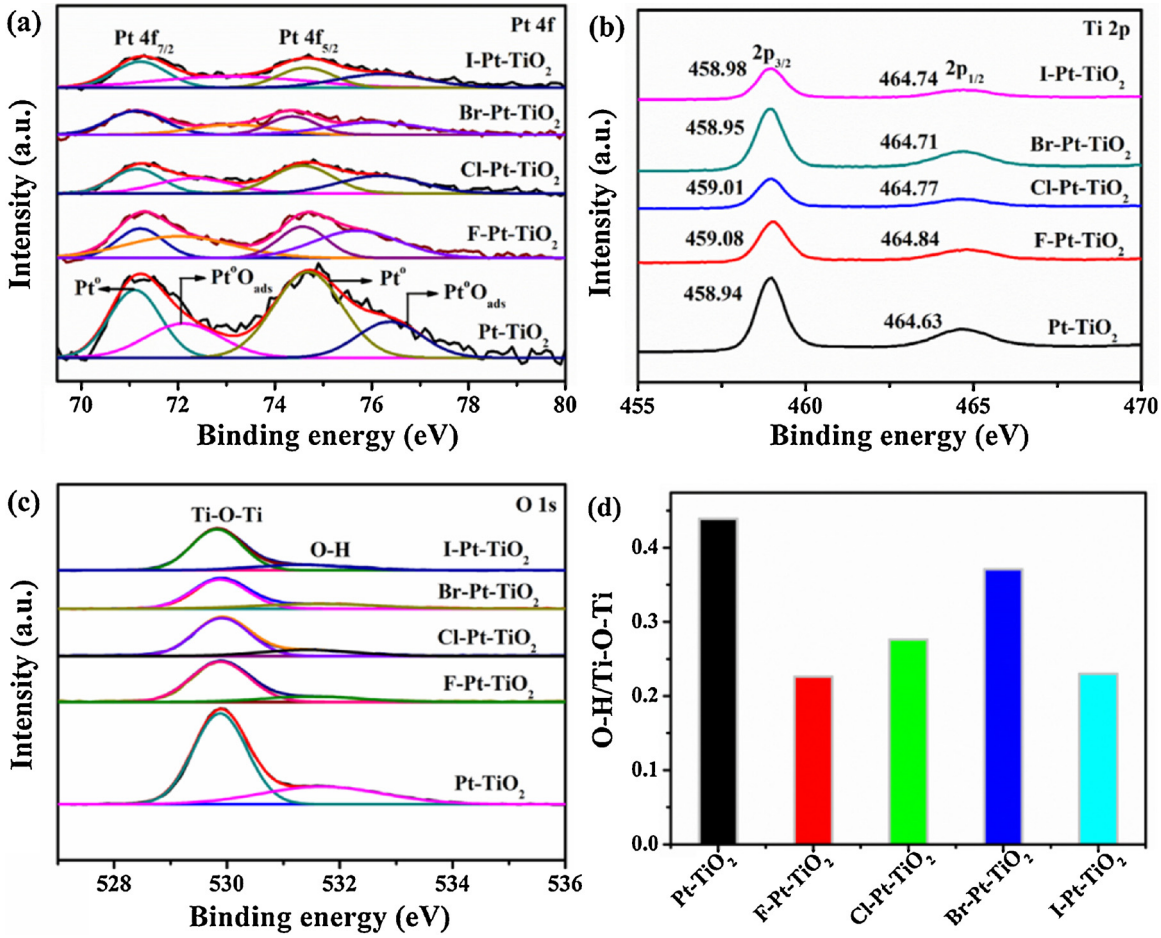

Fig. 8. XPS spectra for (a) Pt 4f, (b) Ti 2p and (c) O 1 s of the Pt-TiO_2, F-Pt-TiO_2, Cl-Pt-TiO_2, Br-Pt-TiO_2, and I-Pt-TiO_2 catalysts. (d) The relative intensity ratio of fitted peaks of the XPS spectra of Pt-TiO_2 and halogen ions adsorbed Pt-TiO_2 for the O 1 s region (the intensity ratio was calculated by the ratio of each peak area to the corresponding total area of oxygen peaks).

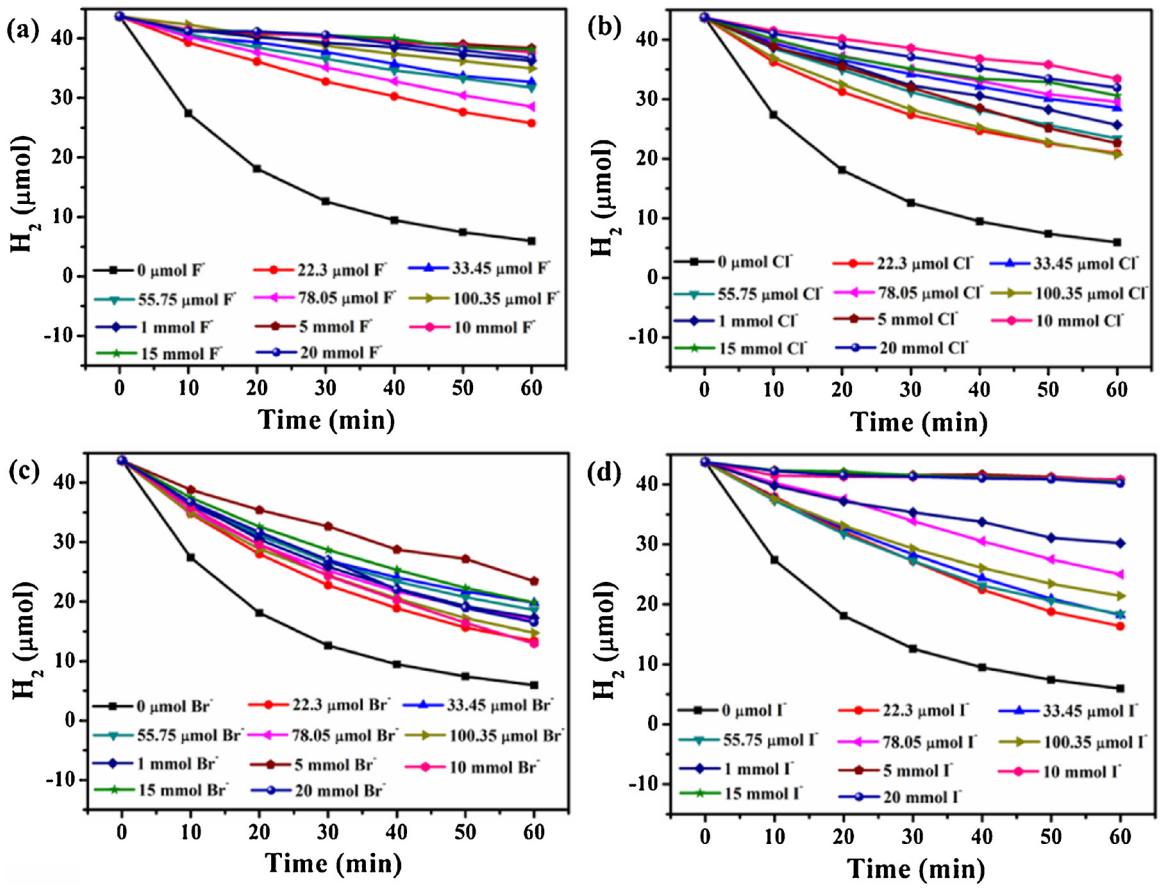

Fig. 9. The H_2 and O_2 recombination reaction for various F-Pt-TiO_2, Cl-Pt-TiO_2, Br-Pt-TiO_2 and I-Pt-TiO_2.

Table 3
H_2 recombination rates for different F-Pt-TiO_2, Cl-Pt-TiO_2, Br-Pt-TiO_2 and I-Pt-TiO_2 catalysts.

Halogen ions amount (μmol)	H_2 recombination rates (min^{-1})			
	F-Pt-TiO_2	Cl-Pt-TiO_2	Br-Pt-TiO_2	I-Pt-TiO_2
0	0.03305	0.03305	0.03305	0.03305
22.3	0.01131	0.02421	0.02977	0.01728
33.45	0.00665	0.00982	0.02671	0.01478
55.75	0.00567	0.01233	0.02367	0.01634
78.05	0.00879	0.01036	0.02412	0.01184
100.35	0.00584	0.01885	0.01864	0.01407
1000	0.00287	0.01372	0.02228	0.00688
5000	0.0028	0.01329	0.01188	0.00105
10000	0.00268	0.00524	0.01762	0.00107
15000	0.00211	0.00795	0.01512	0.00136
20000	0.00251	0.00835	0.01484	0.00191

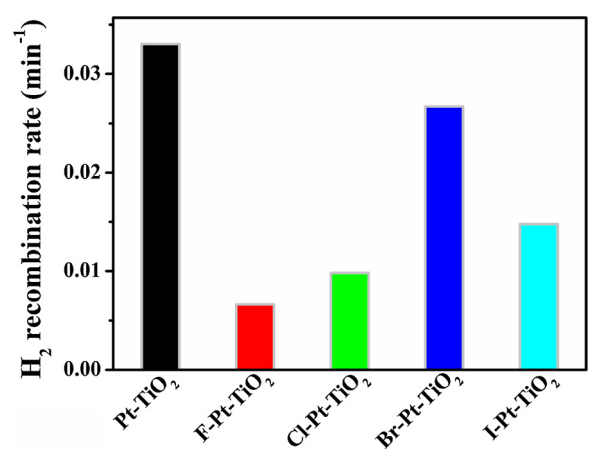

Fig. 10. H_2 and O_2 recombination rates for Pt-TiO_2, F-Pt-TiO_2, Cl-Pt-TiO_2, Br-Pt-TiO_2 and I-Pt-TiO_2 (The amount of halogen ions was 33.45 μmol).

50 mg well dispersed catalyst was degassed by bubbling Ar gas for 30 min. The amount of evolved gas was monitored by gas chromatography (Agilent 6820, TCD, 13 × column, Ar carrier).

2.4. Isotopes tracer experiments

The isotopes tracer experiments were performed in a sealed Pyrex reactor. Typically, 10 mg catalyst was dispersed in 10 mL D_2O or 2 mL $H_2{}^{18}O$ in the sealed Pyrex flask. After ultrasonic treatment for 30 min, the suspended aqueous solution was degassed by bubbling Ar gas for another 30 min. After 3 h UV light irradiation, the gas mixture in container was measured by GC–MS (Agilent Technologies, GC 7890 A with a PONA capillary column (50 m × 0.20 mm × 0.50 μm), MS 5975C, the temperature of sample injector was maintained at 240 °C).

2.5. CV measurements

The cyclic voltammetry (CV) measurement was conducted on a CHI 660E electrochemical workstation (Shanghai CH Instrument Company, China) in a standard three electrode cell. A platinum foil was used as counter electrode and a saturated calomel electrode (SCE) was use as reference electrode. An indium tin oxide glass (ITO glass) was used as a working electrode, which was washed with ethanol and DI water with sonication respectively before the experiments. Sample (6.4 mg) was dispersed into 4 mL distilled water. Aliquots of the solution (40 u L) were removed and dropped onto the precleaned ITO glass with a micropipette. Nafion solution (0.025 wt%, 20 u L) was then dropped onto

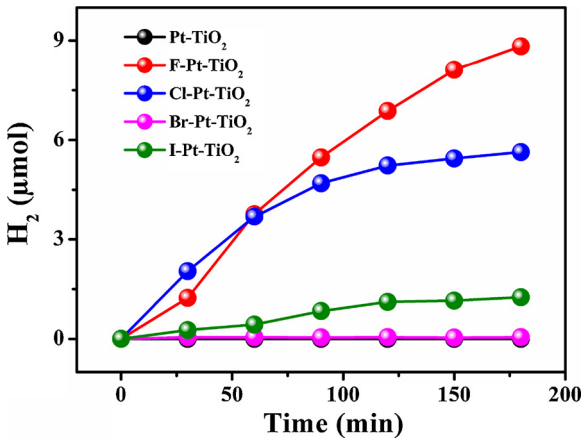

Fig. 11. The time courses of H_2 evolution over Pt-TiO_2 and halogen ions adsorbed Pt-TiO_2 photocatalysts in pure water under irradiation (The amount of halogen ions was 33.45 μmol).

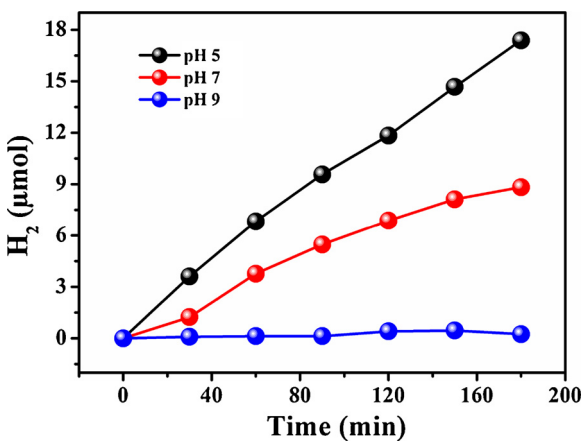

Fig. 12. Effect of pH on photocatalytic activity for F-Pt-TiO_2 catalyst.

Table 4
Parameters of fluorescence decays of Pt-TiO_2, F-Pt-TiO_2, Cl-Pt-TiO_2, Br-Pt-TiO_2 and I-Pt-TiO_2 samples.

Samples	lifetime < τ > (ns)	pre-exponential factors B	average lifetime < τ > (ns)	χ^2
Pt-TiO_2	τ_1 = 0.02	B_1 = 0.8514	2.89	1.03
	τ_2 = 3.09	B_2 = 0.1486		
F-Pt-TiO_2	τ_1 = 6.24	B_1 = 0.2146	6.10	1.30
	τ_2 = 0.04	B_2 = 0.7854		
Cl-Pt-TiO_2	τ_1 = 5.07	B_1 = 0.4775	4.87	1.27
	τ_2 = 0.20	B_2 = 0.5225		
Br-Pt-TiO_2	τ_1 = 0.04	B_1 = 0.7721	4.73	1.19
	τ_2 = 4.86	B_2 = 0.2279		
I-Pt-TiO_2	τ_1 = 0.10	B_1 = 0.6810	4.63	1.00
	τ_2 = 4.83	B_2 = 0.3190		

the electrocatalysts coated electrode and drying at room temperature. The electrolyte (0.5 M H_2SO_4 solution) was firstly bubbled with O_2 for 30 min and then bubbling H_2 for another 30 min. The electrodes were cycled in the potential range between -0.105 and 1.3 V at a scan rate of 10 mV/s after electrochemical cleaning with a quick scan (200 mV/s) for 50 cycles.

2.6. H_2-TPD measurements

H_2-Temperature Programmed Desorption (TPD) experiments were recorded on a thermal conductivity detector (TCD). One hundred mg of the catalyst was dosed with H_2/Ar (5% v/v) to saturation of H_2 adsorption at 35 °C. Subsequently, Argon gas was purged for 2 h to remove weakly adsorbed species. Finally, the catalysts were heated in flowing argon by ramping the temperature from 35 to 400 °C at a rate of 5 °C/min.

2.7. Adsorption energy calculation method

In this study, all the adsorption energy calculations were carried out with the plane-wave density functional theory (DFT) (B3LYP) method performed in the program of Gussian 09 [44]. We used a 6-311G** basis set for the O and H atoms and a LANL2DZ basis set for the Pt atoms [61]. The LANL2DZ basis set, which have been proven to be quite satisfied in the theoretical computations when applied to metallic atoms, was chosen to describe the geometrical structures and the electronic features [62].

The adsorption energy was defined as:

$$E_{ads} = E_{adsorbate/slab} - E_{adsorbate} - E_{slab}$$

where $E_{adsorbate/slab}$ is the total energy of the adsorbate together with the slab, $E_{adsorbate}$ is the total energy of the free adsorbate, and E_{slab} is the total energy of the bare slab [63]. With this definition, the more negative values of adsorption energy imply that adsorption is more stable.

2.8. Characterizations

X-ray diffraction (XRD) patterns of the catalysts were obtained on a Rigaku B/Max-RB X-ray diffractometer with a nickel-filtrated Cu Kα radiation operated at 40 kV and 40 mA. Ultraviolet-visible (UV–vis) diffuse reflectance spectra (DRS) were obtained with a Shimadzu UV-2550 UV–vis spectrophotometer. $BaSO_4$ was used as a reflectance standard. Transmission electron microscopy (TEM) and HRTEM images were conducted with a Tecnai-G2-F30 field emission transmission electron microscope operating at accelerating voltage of 300 kV. X-ray photoelectron spectroscopy (XPS) was performed on a VG Scientific ESCALAB 210-XPS spectrometer system (Al Kα X-ray source). The fluorescence decay times were measured using the Horiba Jobin Yvon Data Station HUB operating in time-correlated single photon counting mode (TCSPC). Nano LED diode emitting pulses at 284 nm was used as an excitation source. Horiba Jobin Yvon DAS6 fluorescence decay analysis software was used to fit the model function to the experimental data.

3. Results and discussion

3.1. DFT studies

In order to identify that the role of halogen ions on the inhibition of H_2 and O_2 recombination reaction on Pt surface, the calculation using plane-wave density functional theory (DFT) method was carried out to determine the adsorption energies of H_2 and O_2 molecule on Pt [44,62–65]. Here, we used a model of Pt_6 (100) cluster to simulate the interactions between hydrogen or oxygen molecule and halogen ions on Pt(100) surface. Figs. 1 and 2 showed the optimized geometries of hydrogen and oxygen molecules adsorbed on Pt_6(100) and halogen ions adsorbed Pt_6(100) cluster. The cluster geometry was fixed according to experimental Pt-Pt distance of 2.77 Å in bulk platinum. The calculated adsorption energies results were summarized in Table 1. On pristine Pt surface, the adsorption energy of H_2 was −0.92 eV. The adsorbed H_2 molecule can easily dissociate into two atomic H. By contrast, molecular adsorption of H_2 on halogen ions pre-adsorbed Pt surface became relatively difficult. Adsorption energies of H_2 were calculated to be as lower as −0.22, −0.47, −0.52, −0.49 eV for F/Pt, Cl/Pt, Br/Pt, I/Pt, respectively. Similarly, O_2 molecule can even directly dissociate into

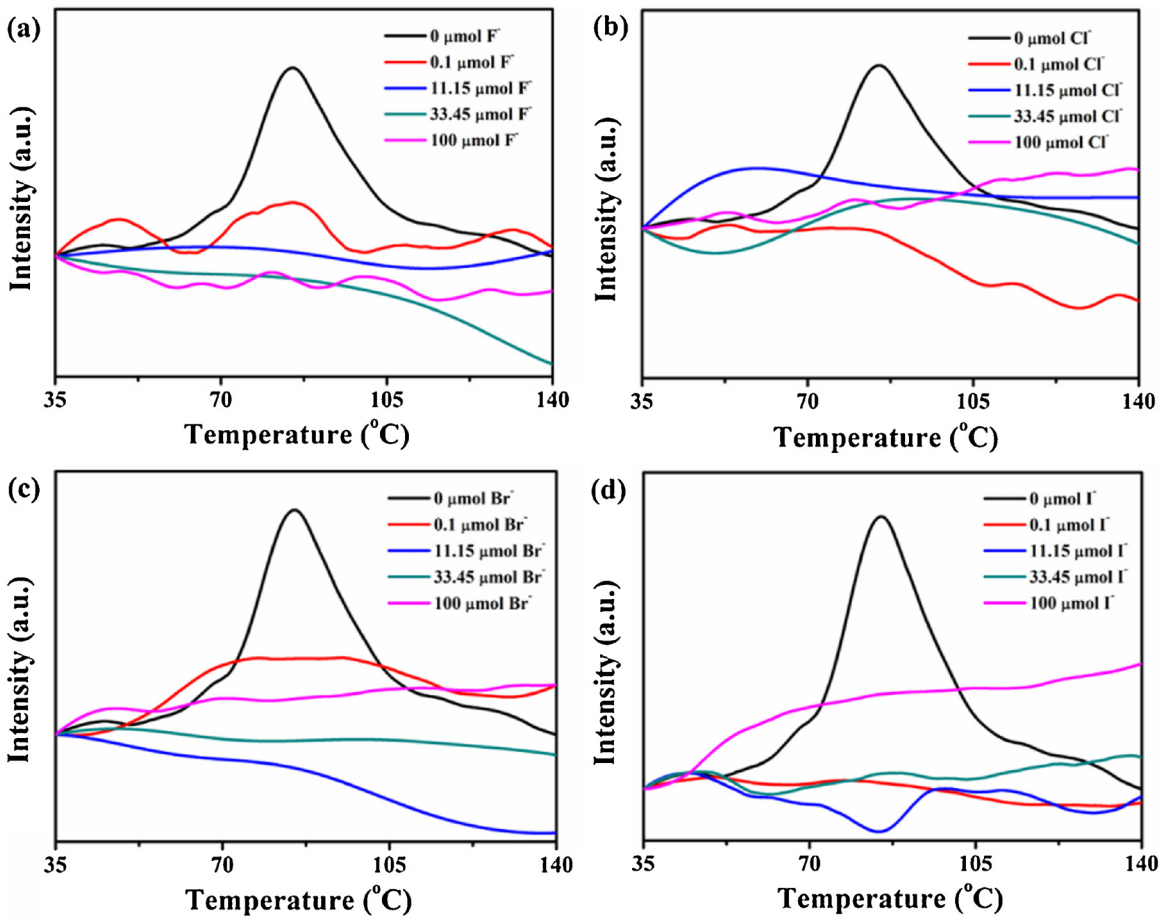

Fig. 13. H_2-TPD of Pt-TiO_2, F-Pt-TiO_2, Cl-Pt-TiO_2, Br-Pt-TiO_2, and I-Pt-TiO_2 catalysts.

two atomic O with adsorption energy of −1.67 eV over Pt. However, the adsorption energies of O_2 for F/Pt, Cl/Pt, Br/Pt, I/Pt decreased to −1.21, −1.38, −1.43, −1.39 eV, therefore adsorption of O_2 on halogen ions adsorbed Pt surface also became difficult. Thus, the halogen ions pre-adsorbed Pt catalysts presented significant inhibition ability compared to pristine Pt in activating H_2 into atomic H or activating the O_2 molecule. Calculation results revealed that the adsorption energies of H_2 and O_2 over halogen atoms pre-adsorbed Pt catalysts followed the order of F/Pt < Cl/Pt < I/Pt < Br/Pt < Pt.

To investigate the influence of the nature of halogen ions on hydrogen and oxygen adsorption on Pt, we adopt the relatively larger Pt_8 (100) cluster model as the substrate, and toke the fluorine ion as a representative halogen ions. Fig. 3a showed the H_2 molecule adsorbed on the clean Pt_8 (100) cluster with the calculated adsorption energy of −1.14 eV (see Table 2). When a fluorine ion adsorbed the Pt 1 top site (Fig. 3b), the adsorption energy of H_2 molecule decreased to −0.65 eV. By contrast, the H_2 adsorption energy with fluorine ion on the Pt 2 top site was −0.77 eV (Fig. 3c). It was also found that the adsorption energy of H_2 molecule decreased to −0.32 eV when the Pt 1 and Pt 2 top sites were both adsorbed with fluorine ions (Fig. 3d). The calculation results demonstrated that H_2 adsorption energy was significant affected by the nearest adsorbed fluorine ion, while was less influenced by the more distance one. The more fluorine ions adsorbed on Pt surface corresponded to the lower adsorption energy of hydrogen molecules. The similar dependence was found in the cases of O_2 adsorption (see Fig. 4 and Table 2).

3.2. XRD analysis

Based on the analysis of DFT calculations, a series of halogen ions pre-adsorbed Pt-TiO_2 catalysts were prepared by impregnation and ion modification methods. The XRD patterns of the as-prepared catalysts were shown in Fig. 5. For these samples, the peaks at 2θ diffraction angles of 25.3, 37.9, 48.2, 54.1, 55, 62.6, 69, 70.3, 75° were indexed as (101), (004), (200), (105), (211), (204), (116), (220) and (215) crystal planes of anatase TiO_2. In addition, the peaks at 27.5, 36, 41.2° were indexed as (110), (101) and (111) crystal planes of rutile TiO_2 [66,67]. These results indicated that the adsorption of halogen ions did not change the phase structure of the catalysts. No diffraction peaks of Pt were observed, which might be ascribed to the low content and highly dispersed on the catalyst surface [68].

3.3. Morphology analysis

TEM and HRTEM results were displayed in Fig. 6, confirming the existence of TiO_2 nanosheets and Pt nanoparticles (NPs). The TEM images of Pt-TiO_2, F-Pt-TiO_2, Cl-Pt-TiO_2, Br-Pt-TiO_2, and I-Pt-TiO_2 (Fig. 6a–e) showed that many small Pt nanoparticles were deposited on the surface of TiO_2 nanosheets. The energy dispersive X-ray spectroscopy (EDS) measurements (inset of Fig. 6a–e) confirmed the presence of titanium, oxygen, platinum elements on Pt-TiO_2 catalysts, and the fluorine, chlorine, bromine, iodine elements in the F-Pt-TiO_2, Cl-Pt-TiO_2, Br-Pt-TiO_2, and I-Pt-TiO_2 catalysts, respectively. Fig. 6f–j showed the high-magnified micrographs of Pt-TiO_2, F-Pt-TiO_2, Cl-Pt-TiO_2, Br-Pt-TiO_2, and I-Pt-TiO_2 catalysts. As seen in Fig. 6f–j, the lattice fringes exhibit the typical distances for the anatase phase, for instance, TiO_2(101) (0.35 nm). The lattice spacing of 0.2 nm could be assigned to the (200) facet of Pt nanoparticles, which was equivalent to the (100) facet. The selected area electron diffraction (SAED) patterns (inset of Fig. 6f–j) further confirmed the (101) plane of the crystal structure of

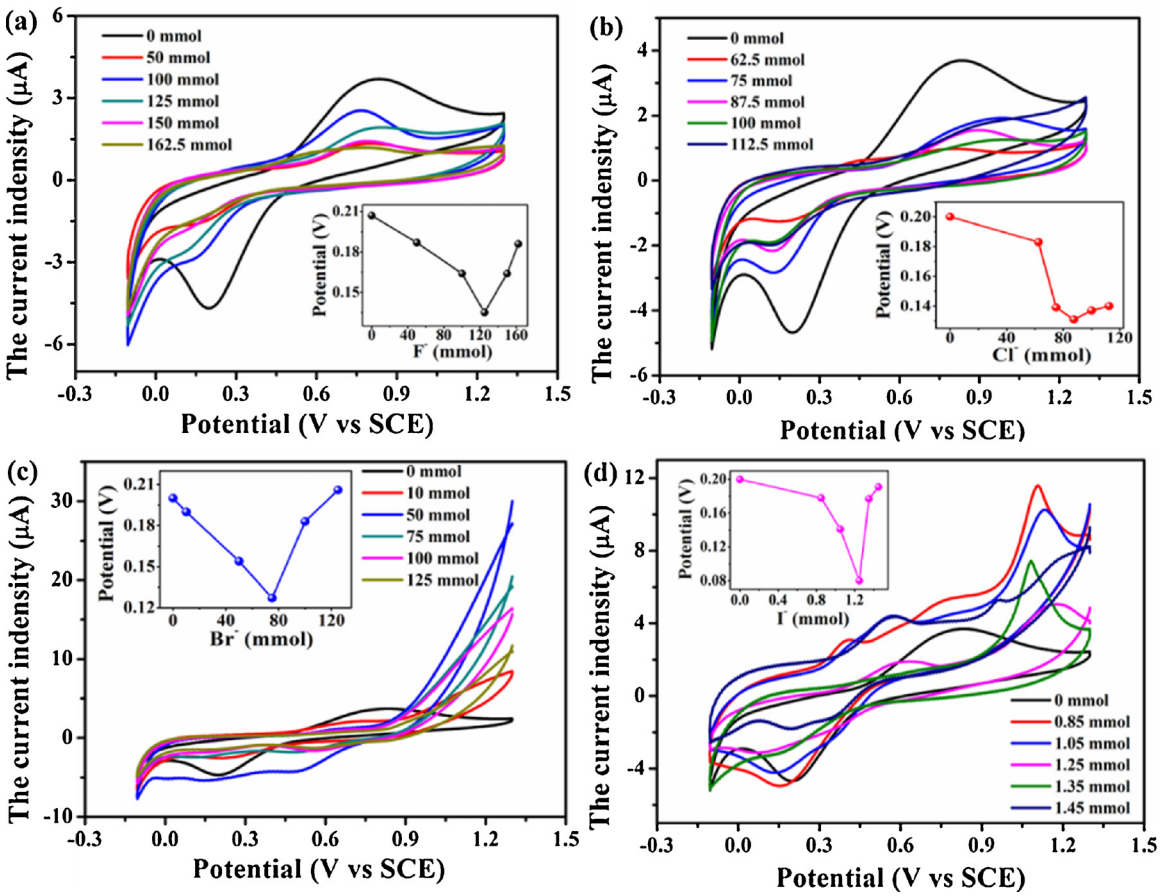

Fig. 14. CVs of the Pt-TiO_2 catalyst with adding different amounts of (a) fluorine ion, (b) chlorine ion, (c) bromine ion, (d) iodine ion on ITO glass in 0.5 M H_2SO_4 solution by feeding O_2 and H_2. Sweep rate: 10 mV/s. Inset shows the cathodic peak potentials as a function of F^-, Cl^-, Br^-, I^- content, respectively.

titanium dioxide and the (200) facet of the crystal structure of platinum. Fig. 7 clearly showed that the Pt, Ti, O elements and the corresponding F, Cl, Br, I elements were relatively homogeneous distributed in the halogen/Pt-TiO_2 photocatalysts.

3.4. XPS analysis

X-ray photoelectron spectroscopy (XPS) was used to obtain the composition and chemical states of elements according to their binding energies in the as-synthesized catalysts. The XPS spectra of F 1 s, Cl 2p, Br 3d, and I 3d regions were provided in Fig. S1. In Fig. S1a, the binding energy of 684.23 eV corresponds to F 1 s in the F-Pt-TiO_2. Similarly, the Cl $2p_{3/2}$ and Cl $2p_{1/2}$ peaks at 197.96 and 199.50 eV, the Br $3d_{5/2}$ and Br $3d_{3/2}$ peaks at 67.98 and 69.01 eV, and the I $3d_{5/2}$ and I $3d_{3/2}$ peaks at 618.60 and 629.96 eV were observed in Fig. S1b-d, respectively [69]. No other peaks were observed in each spectrum, which indicated that fluorine, chlorine, bromine, iodine ions were mainly adsorbed on the Pt-TiO_2 surface.

In Fig. 8a, the Pt 4f spectra of Pt-TiO_2 showed Pt $4f_{7/2}$ peaks located at 71.11 and 72.12 eV, and Pt $4f_{5/2}$ peaks located at 74.67 and 76.40 eV. One couple of the peaks at 71.11 and 74.67 eV were ascribed to Pt^o, while the other couple of peaks at 72.12 and 76.40 eV were ascribed to Pt^oO_{ads} (Pt^oO_{ads} is metallic Pt with surface adsorbed oxygen) [70]. The strong electronegativity of halogen ions leads to electron transfer from Pt to halogen, the binding energies of Pt^o for F-Pt-TiO_2 (71.22 eV), Cl-Pt-TiO_2 (71.17 eV), Br-Pt-TiO_2 (71.14 eV) and I-Pt-TiO_2 (71.23 eV) showed slight high energy shift as compared to Pt-TiO_2 (71.11 eV). Similarly, the weak positive shifts of Ti binding energy were also observed (Fig. 8b), due to the highly electronegative halogen induced electron transfer [71]. Fig. 8c illustrated the XPS peaks of O 1 s for the Pt-TiO_2 and halogen ions adsorbed Pt-TiO_2 catalysts. The wide shape and asymmetric peaks of O 1 s spectra demonstrated the presence of more than one chemical states according to the binding energy data [72,73]. It corresponded to the crystal lattice oxygen ($O_{Ti\text{-}O\text{-}Ti}$), and surface hydroxyl groups ($O_{O\text{-}H}$) on the surface of TiO_2 NPs with increasing binding energy [74–76]. Base on the XPS results, the ratios of $O_{O\text{-}H}/O_{Ti\text{-}O\text{-}Ti}$ were determined to be 0.439, 0.226, 0.276, 0.371, 0.23 for Pt-TiO_2, F-Pt-TiO_2, Cl-Pt-TiO_2, Br-Pt-TiO_2, I-Pt-TiO_2, respectively (Fig. 8d). The results illustrated that adsorption of halogen ions could lower the relative intensity of hydroxyl oxygen on TiO_2 surface.

It was reported that the surface fluorination would induce the typical ligand exchange reaction, which was the replacement the surface hydroxyl groups by fluorine ion on TiO_2 [77,78].

$$\equiv Ti-OH + F^- \rightarrow \equiv Ti\text{-}F + OH\text{-} \quad (1)$$

Similarly, chlorine, bromine and iodine atoms could replace the OH groups on TiO_2, and then decrease of oxygen ratio was observed. In addition, the fluorine atom cannot replace oxygen atom in TiO_2 to influence the crystalline phase of bulk TiO_2 [79].

3.5. Catalytic activity test

3.5.1. H_2 and O_2 recombination reaction

The H_2 and O_2 recombination reaction over Pt-TiO_2 catalysts pre-adsorbed with different amounts of F^-, Cl^-, Br^-, I^- were measured and the results were presented in Fig. 9a-d, respectively. It was shown that the concentration of H_2 decreased remarkably with the time over the Pt-TiO_2 catalyst. When the halogen ions were adding into the Pt-TiO_2 catalysts, the amount of recombined H_2 decreased over all of the halogen pre-adsorbed catalysts. Adsorption of halogen ions could

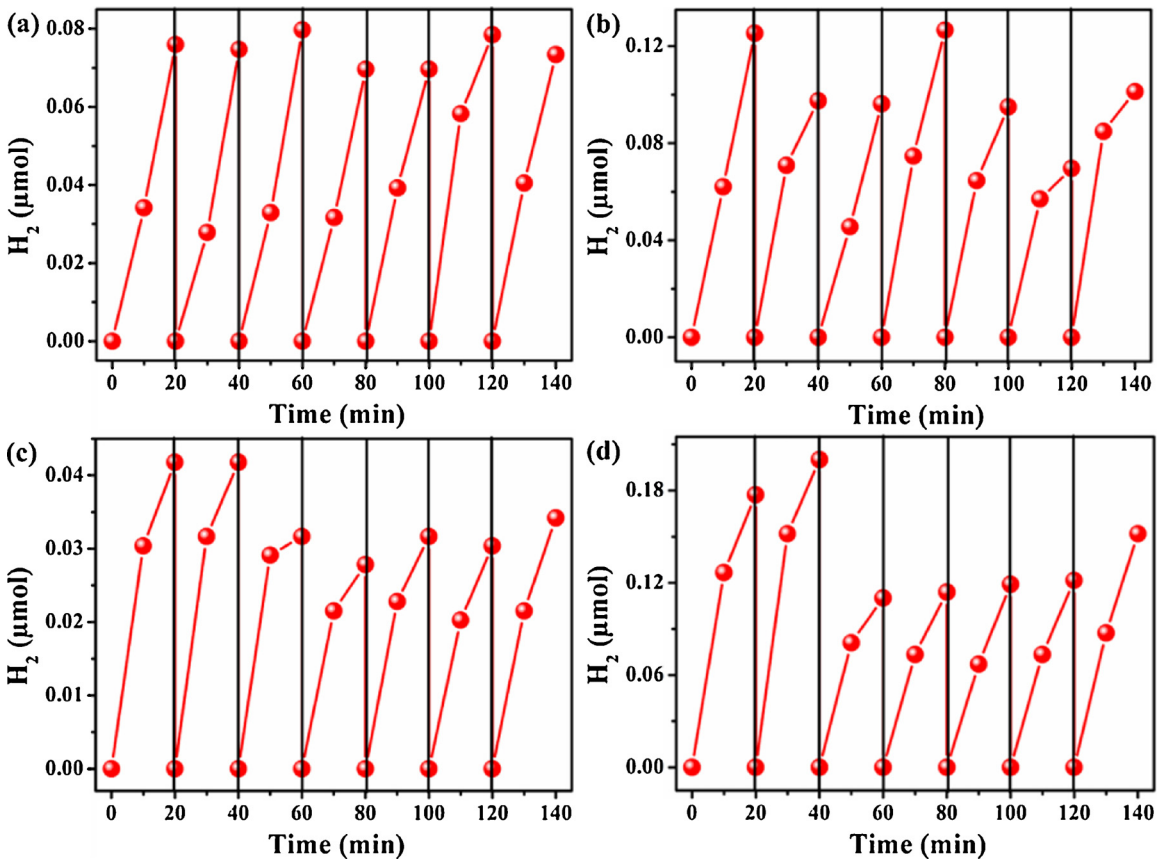

Fig. 15. Cycle performance of the photocatalytic activity for various samples: (a) F-Pt-TiO_2, (b) Cl-Pt-TiO_2, (c) Br-Pt-TiO_2, (d) I-Pt-TiO_2.

obviously inhibit the H_2 and O_2 recombination reaction. Table 3 present the corresponding H_2 recombination rates for the Pt-TiO_2 catalysts with adding different amounts of F^-, Cl^-, Br^-, I^-, respectively. Results indicated that the H_2 recombination rates decreased with increasing halogen concentration in the low concentration range, but the decrease tendency became weak in the high halogen ions concentration range. In order to compare the inhibited ability for different halogen ions, the results of H_2 recombination rates for Pt-TiO_2 catalysts with the same amount of halogen ions were presented in Fig. 10. Clearly, the H_2 recombination rates for different catalysts followed the order of F-Pt-TiO_2 < Cl-Pt-TiO_2 < I-Pt-TiO_2 < Br-Pt-TiO_2 < Pt-TiO_2. The H_2 and O_2 recombination results were well consistent with the above DFT calculation.

3.5.2. Hydrogen evolution activity

The reaction time courses of H_2 evolution over Pt-TiO_2, F-Pt-TiO_2, Cl-Pt-TiO_2, Br-Pt-TiO_2, I-Pt-TiO_2 photocatalysts in pure water were shown in Fig. 11. It was found that no H_2 was evolved over Pt-TiO_2 photocatalyst in pure water under irradiation. After pre-adsorbed small amount of halogen ions (33.45 μmol) on Pt-TiO_2 photocatalyst, the H_2 generation were achieved and the amounts of H_2 generated was 8.83, 5.63, 0.05, 1.25 μmol in 3 h over F-Pt-TiO_2, Cl-Pt-TiO_2, Br-Pt-TiO_2, I-Pt-TiO_2 catalysts, respectively. Results indicated that the H_2 and O_2 recombination reverse reaction was effectively inhibited and the photocatalytic over-all water splitting was achieved.

The effects of pH on activities of halogen ions adsorbed Pt-TiO_2 catalyst were investigated. Taken the F/Pt-TiO_2 catalyst as an example (shown in Fig. 12), we found that the hydrogen evolution activity was dependent on the reaction pH. The activity for the F-Pt/TiO_2 photocatalyst was gradually decreased with increasing the pH value from 5 to 9. The similar activities dependence on pH were observed over other halogen ion adsorbed Pt/TiO_2 catalysts (see Fig. S3). In general, pH variation will significantly affect the F adsorption on TiO_2 [80] due to the variation of charged surface environment. In the pH 5 solution, the TiO_2 surface is weak positively charged, while in the pH 9 solution, the TiO_2 surface is weak negatively charged. The stronger interaction between F and TiO_2 will take place in the former low pH environment, which makes negative fluorine ions exhibit more significantly inhibition effect on reverse recombination reaction of hydrogen and oxygen in the former situation. In order to confirm this assumption, the reverse recombination rates of hydrogen and oxygen over F-Pt/TiO_2 were measured under different pH conditions. As results shown in Fig. S2 and Fig. S3, the recombination rates over F-Pt/TiO_2 catalyst increased with increasing the pH. In fact, when the catalyst surface was negatively charged at pH 9, the adsorption of fluorine ions became difficult due to an electrostatic repulsive force [81]. Besides, the pH will also affect the hydrogen generation activity of Pt/TiO_2 because the flatband of TiO_2 change when pH varied. The hydrogen evolution reaction prefer acidic environment.

Fluorescence lifetime measurements were also carried out and the results were shown in Table 4. Apparently, the average lifetimes of photo-generated charges of all the halogen ions adsorbed Pt-TiO_2 catalysts were higher than that of Pt-TiO_2 catalyst, which indicated that the halogen ions could efficiently prolong the lifetime of charge carriers and inhibit the electron-hole recombination. It has been reported that the surface fluorination could removal the surface hydroxyl groups by fluoride substitution, and thus hinder the surface hole trapping and enhance the hole transfer to H_2O molecules [82]. As a result, direct recombination CB electrons and the holes were minimized. Similarly, chlorine, bromine and iodine ions could also hinder the surface hole trapping, and inhibit the electron-hole recombination. Our results indicated that the adsorbed halogen ions can not only decrease the H_2 and O_2 recombination, but also improve the separation and transfer of photogenerated charges and eventually enhance the higher

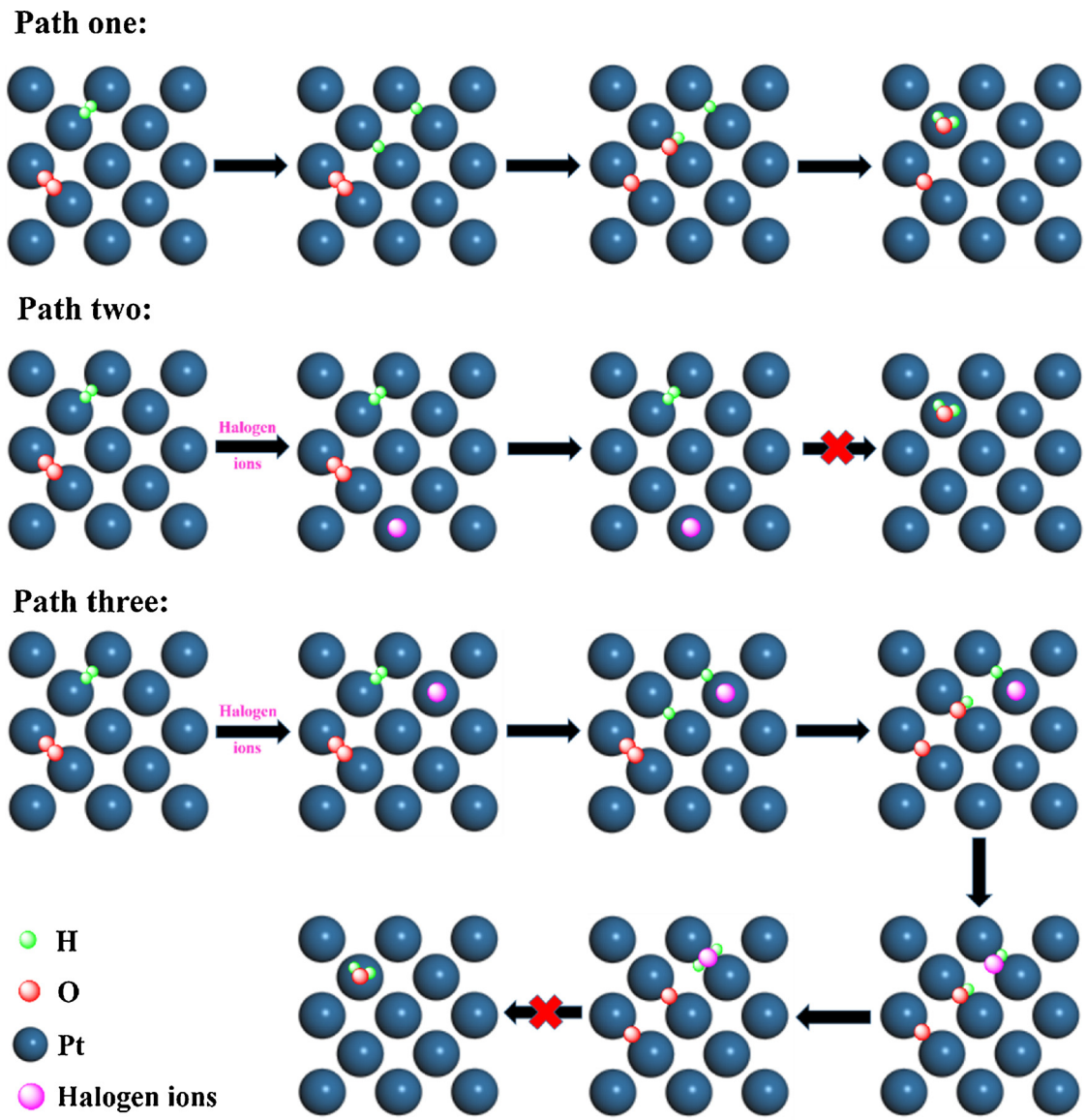

Scheme 1. Schematic of the H_2 and O_2 recombination process and the possible mechanism of halogen ions inhibition on H_2 and O_2 recombination over Pt(100) surface.

photocatalytic performance.

3.6. Isotopes tracer experiments

To further confirm that H_2 and O_2 were simultaneously generated via water splitting over halogen ions adsorbed Pt-TiO_2 catalysts the isotopic tracer experiments were carried out. As results displayed in Fig. S4a, the *m/z* signal of 4 corresponded to the D_2, indicating that D_2 formation from D_2O splitting over F-Pt-TiO_2. In Fig. S4b, the *m/z* signal of 36 corresponding to the $^{18}O_2$ was detected, confirming that $^{18}O_2$ was from $H_2{}^{18}O$. Those isotopes tracer experiments identified that the halogen ions adsorbed Pt-TiO_2 catalysts could catalyze overall water splitting to hydrogen and oxygen.

3.7. H_2-TPD

The H_2 adsorption types and amounts over Pt-TiO_2, F-Pt-TiO_2, Cl-Pt-TiO_2, Br-Pt-TiO_2, and I-Pt-TiO_2 catalysts were studied by H_2-TPD and the results were shown in Fig. 13. H_2 desorption peaks centered at 85 °C for all the catalysts were due to chemisorbed hydrogen on the surface of Pt surface [83]. As shown in Fig. 13a–d, the intensities of H_2 desorption peaks on Pt-TiO_2 catalysts decreased with the addition of halogen ions. These phenomena confirmed that adsorption of halogen ions on the Pt-TiO_2 catalyst indeed lowered the adsorption of hydrogen molecules on the Pt surface, due to their strong electronegativity and priority to occupy the surface sites of Pt. However, adding too much halogen ions might lead to multi-layer occupation of halogen ions on the Pt surface, and decreased the amount of chemisorbed state of them.

3.8. Cyclic voltammetry

Fig. 14 illustrated the cyclic voltammograms obtained from Pt-TiO_2 catalysts with adding different amounts of halogen ions. The redox peaks of Pt-TiO_2 catalysts located at 0.20 eV were peaks from the hydrogen and oxygen recombination. As results shown in Fig. 14a, the recombination peaks shift to the lower potential side with the amount of fluorine ion increasing when the F^- content was lower than 125 mmol, and then shift to the high potential side when the F^- concentration further increases (see the inset of Fig. 14a). Similar variation tendency has been observed for Pt-TiO_2 catalysts with adding other halogen ions (Fig. 14b–d). Due to the strong electronegativity, the adsorption of halogen ions would lead to more difficult hydrogen and

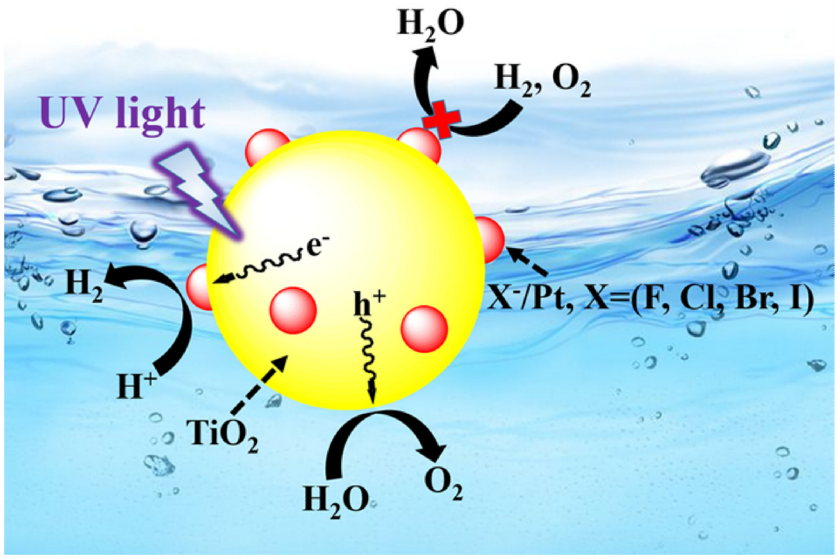

Scheme 2. Schematic illustration of mechanism of UV-light-driven overall water splitting on halogen ions adsorbed Pt-TiO_2 catalysts.

oxygen adsorption. As a result, the recombination peaks shifted to the lower potentials and the H_2 and O_2 recombination reaction hardly occurred. However, as the H_2-TPD analysis showing, over loading halogen ions might lead to multi-layer occupation state of halogen ions on Pt surface, and then decreased their inhibition effects.

It was also found that the concentration of halogen ions corresponding to the lowest potential of the reduction peaks were quite different. As results shown in Fig. 14 and S5, the lowest potential of the reduction peaks appeared at different concentrations of halogen ions over tested samples, and that potential gradually decreased from fluorine ions to iodine ions. Since the halogen ions adsorption on the catalyst surface was mainly determined by strong electronic interaction, the adsorption ability of halogen ions on Pt surface decreased from F to I since the electronegativity of halogen ions were gradually decreased from F to I. In addition, the increased radius of the halogen ions also resulted in the increased steric hindrance, which would lead to the weaker monolayer adsorption of halogen ions on Pt surface from F to I. Therefore, increasing halogen ions concentration would shift such adsorption to multi-layer adsorption. As a result, the concentration of halogen ions corresponding to the lowest potential of the reduction peaks was gradually decreased. In fact, the iodine ions present the smallest electronegativity and the largest radius, corresponding to the weaker chemical adsorption ability and the stronger steric hindrance effect.

3.9. Stability test

The stability of the photocatalytic water splitting performance over halogen ions adsorbed Pt-TiO_2 catalysts were examined (Fig. 15). It displayed that the all the catalysts showed pretty stable performance during the cycle photocatalytic reactions. However, slightly decreased photocatalytic activities were also observed over some catalysts, for example, bromine ions and iodine ions adsorbed Pt-TiO_2. This might ascribed to the changes of adsorption site and adsorbed state of Br and I, or catalyst lose and segregation during the following cycle experiments, although the detail understanding of such changes are still unknown and waiting for much more hyperfine-designed investigations.

3.10. Inhibition mechanism of H_2 and O_2 recombination

As depicted in Scheme 1 on clean Pt(100) surface, the H_2 and O_2 molecule adsorbed at the bridge sites in the initiate state (path one). Then, the adsorbed H_2 dissociated through the transition state with H atoms chemisorbed at two separate bridges sites [61]. Then, the O_2 molecule breaks into two O atoms, which were also chemisorbed at the bridge sites. The atomic H migrating across a hollow site to the nearby atomic O, and OH molecule formed at the bridge site. The OH molecule rotated on the surface and moved to a nearby top site, while the H atom moved toward the OH molecule. Finally, the H_2O molecule was formed at the top site [84]. This step was followed by the water desorption from the Pt surface.

Nevertheless, the chemical environment around the metallic platinum would change when halogen ions adsorbed on the Pt surface. According to the H_2-TPD and DFT analysis, both the experimental and theoretical studies demonstrated that the adsorption of halogen ions on Pt surfaces could lower the adsorption energies of H_2 and O_2 molecules. The strong electronegativity of halogen would induce the electron transfer from Pt to halogen ions. Consequently, the electron density of metallic platinum would decrease, and lead to the decrease of the adsorption and activation of H_2 and O_2 on Pt surface. Based on above analysis, we speculate the possible mechanism of halogen ions inhibition of the H_2 and O_2 recombination reaction as follows. H_2 and O_2 molecule were first adsorbed on Pt surface. When the halogen ion was pre-adsorbed onto the Pt-TiO_2 catalyst, the halogen ions prefer occupied the top Pt site [85]. As a result, the adsorption of the O_2 molecule on Pt surface was impeded according to the DFT calculation results. The H_2 cannot react with O_2 to form water in the absence of O_2, therefore, the hydrogen and oxygen recombination was inhibited. Similarly, the adsorption of H_2 molecule would also be impeded on nearby surface site pre-adsorbed by halogen ions, thereby the backward reaction was suppressed.

The possible reaction process of photocatalytic overall water splitting over the halogen ions adsorbed Pt-TiO_2 catalysts under illumination was illustrated in Scheme 2. The TiO_2 absorbed UV light to generate electrons and holes. Subsequently, the electrons transfer to the Pt nanoparticles and reduce H^+ to form H_2, and the holes oxidize the H_2O to form oxygen. The generated H_2 and O_2 would recombine rapidly to form H_2O on the pristine Pt surface if no halogen ions were on catalyst

surface. The overall water splitting could be achieved unless the reverse reaction of water formation from H_2 and O_2 is inhibited.

4. Conclusions

In summary, an effective method for inhibition of H_2 and O_2 recombination reaction on Pt was developed by halogen ions pre-adsorbed on photocatalyst surface in over-all water splitting. DFT calculation and H_2-TPD experiments revealed that the halogen ions could decrease the adsorption energies of H_2 and O_2 molecule on Pt surface, and thereby inhibited the adsorption and activation of nascent formed H_2 and O_2 molecules on catalyst surface. The inhibition of reverse reaction on different catalysts followed the order of F-Pt-TiO_2 > Cl-Pt-TiO_2 > I-Pt-TiO_2 > Br-Pt-TiO_2 > Pt-TiO_2. The spatial occupation of halogen atoms on Pt determined their roles on H_2 and O_2 recombination. By inhibition of reverse reaction, the overall water splitting has been achieved over Pt-TiO_2 photocatalyst. Isotope experiments with D_2O and $H_2{}^{18}O$ confirmed the over-all water splitting into H_2 and O_2. This work may provide new insight of suppressing the H_2 and O_2 recombination reaction and develop high efficient catalysts for over-all water splitting.

Acknowledgment

The authors are thankful for the support of NSFC (Grant Nos. 21433007 and 21673262).

Appendix A. Supplementary data

Supplementary material related to this article can be found, in the online version, at doi:https://doi.org/10.1016/j.apcatb.2018.05.031.

References

[1] J. Wang, Y. Gao, D. Chen, J. Liu, Z. Zhang, Z. Shao, F. Ciucci, ACS Catal. 8 (2017) 364–371.
[2] W.Y. Zhang, W. Gao, X.Q. Zhang, Z. Li, G.X. Lu, Appl. Surf. Sci. 434 (2018) 643–668.
[3] Z.X. Huang, Y.F. Li, Y.X. Li, S.Q. Peng, J. Mol. Catal.(China) 31 (2017) 181–187.
[4] W. Gao, W.Y. Zhang, B. Tian, W.L. Zhen, Y.Q. Wu, X.Q. Zhang, G.X. Lu, Appl. Catal. B 224 (2018) 553–562.
[5] X.Q. Zhang, B. Tian, W.L. Zhen, Z. Li, Y.Q. Wu, G.X. Lu, J. Catal. 354 (2017) 258–269.
[6] X.Q. Zhang, B. Tian, W.L. Zhen, Z. Li, Y.Q. Wu, G.X. Lu, J. Catal. 352 (2017) 572–578.
[7] Z. Li, C. Kong, G.X. Lu, Int. J. Hydrogen Energy 40 (2015) 9061–9068.
[8] Z. Li, Q.S. Wang, C. Kong, G.X. Lu, J. Phys. Chem. C 119 (2015) 13561–13568.
[9] C. Kong, Z. Li, G.X. Lu, Int. J. Hydrogen Energy 40 (2015) 5824–5830.
[10] W.Y. Zhang, C. Kong, G.X. Lu, Chem. Commun. 51 (2015) 10158–10161.
[11] Q.Y. Li, G.X. Lu, J. Mol. Catal. A 266 (2007) 75–79.
[12] Y.Q. Wu, G.X. Lu, S.B. Li, J. Photochem. Photobiol. A 181 (2006) 263–267.
[13] K. Liang, L. Guo, K. Marcus, S. Zhang, Z. Yang, D.E. Perea, L. Zhou, Y. Du, Y. Yang, ACS Catal. 7 (2017) 8406–8412.
[14] Q.L. Zhou, L. Li, C.L. Yang, Y.Z. Jiao, X.Y. Zhang, J. Mol. Catal. (China) 31 (2017) 239–246.
[15] B. Tian, W. Gao, X.Q. Zhang, Y.Q. Wu, G.X. Lu, Appl. Catal. B 221 (2018) 618–625.
[16] Z. Li, B. Tian, W.L. Zhen, W.Y. Zhang, Y.Q. Wu, G.X. Lu, Appl. Catal. B 219 (2017) 501–510.
[17] W.L. Zhen, W.J. Jiao, Y.Q. Wu, H.W. Jin, G.X. Lu, Catal. Sci. Tech. 7 (2017) 5028–5037.
[18] W. Gao, W. Zhang, G. Lu, Appl. Catal. B 212 (2017) 23–31.
[19] Z. Li, B. Tian, W.Y. Zhang, X.Q. Zhang, Y.Q. Wu, G.X. Lu, Appl. Catal. B 204 (2017) 33–42.
[20] B. Tian, W.L. Zhen, H.B. Gao, X.Q. Zhang, Z. Li, G.X. Lu, Appl. Catal. B 203 (2017) 789–797.
[21] X.Q. Zhang, G.X. Lu, Carbon 108 (2016) 215–224.
[22] P. He, Y. Chen, W.F. Fu, J. MOl. Catal. (China) 30 (2016) 269–275.
[23] X. Ning, J. Li, B. Yang, W. Zhen, Z. Li, B. Tian, G. Lu, Appl. Catal. B 212 (2017) 129–139.
[24] Y. Pi, Q. Shao, P. Wang, J. Guo, X. Huang, Adv. Funct. Mater. 27 (2017) 1700886–1700894.
[25] W.Y. Zhang, S.L. Yang, J. Li, W. Gao, Y.B. Deng, W.P. Dong, C.J. Zhao, G.X. Lu, Appl. Catal. B 206 (2017) 89–103.
[26] W.L. Zhen, J.T. Ma, G.X. Lu, Appl. Catal. B 190 (2016) 12–25.
[27] Z. Li, C. Kong, G.X. Lu, J. Phys. Chem. C 120 (2016) 56–63.
[28] W.Y. Zhang, C. Kong, W. Gao, G.X. Lu, Chem. Commun. 52 (2016) 3038–3041.
[29] G. Cui, W. Wang, M. Ma, J. Xie, X. Shi, N. Deng, J. Xin, B. Tang, Nano Lett. 15 (2015) 7199–7203.
[30] P. Liu, J.C. Lu, D.K. Chen, F. Liu, J.P. Liu, J. Yu, K.Z. Chen, Y.M. Luo, J. Mol. Catal. (China) 30 (2016) 480–495.
[31] W. Zhen, X. Ning, B. Yang, Y. Wu, Z. Li, G. Lu, Appl. Catal. B 221 (2018) 243–257.
[32] C. Kong, S.X. Min, G.X. Lu, Chem. Commun. 50 (2014) 9281–9283.
[33] Q. Lu, C.L. Li, F. Wang, Q.J. Ren, Z. Ren, J. Mol. Catal. (China) 30 (2016) 557–565.
[34] G. Lu, B. Tian, J. Mol. Catal. (China) 31 (2017) 101–104.
[35] G. Lu, W. Zhen, J. Mol. Catal. (China) 31 (2017) 299–304.
[36] W.Y. Zhang, G.X. Lu, Catal. Sci. Technol. 6 (2016) 7693–7697.
[37] G. Lu, W. Zhang, J. Mol. Catal. (China) 31 (2017) 401–410.
[38] G. Lu, S. Li, Int. J. Hydrogen Energ. 17 (1992) 767–770.
[39] Y. Xin, X. Kan, L.Y. Gan, Z. Zhang, ACS Nano 11 (2017) 10303–10312.
[40] R.K. Singha, A. Shukla, A. Sandupatla, G. Deo, R. Bal, J. Mater. Chem. A 5 (2017) 15688–15699.
[41] Y. Cao, M. Lu, J. Fang, L. Shi, D. Zhang, Chem. Commun. 53 (2017) 7549–7552.
[42] M. Serban, M. Lewis, C. Marshall, R. Doctor, Energ. Fuel 17 (2003) 705–713.
[43] J. Vecchietti, A. Bonivardi, W. Xu, D. Stacchiola, J.J. Delgado, M. Calatayud, S.E. Collins, ACS Catal. 4 (2014) 2088–2096.
[44] H. Gao, W. Zhen, J. Ma, G. Lu, Appl. Catal. B 206 (2017) 353–363.
[45] Z. Li, B. Tian, W. Zhen, Y. Wu, G. Lu, Appl. Catal. B 203 (2017) 408–415.
[46] X. Ning, W. Zhen, Y. Wu, G. Lu, Appl. Catal. B 226 (2018) 373–383.
[47] Z. Li, Y. Wu, G. Lu, Appl. Catal. B 188 (2016) 56–64.
[48] B. Tian, B. Yang, J. Li, Z. Li, W. Zhen, Y. Wu, G. Lu, J. Catal. 350 (2017) 189–196.
[49] M. Wang, Z. Li, Y. Wu, J. Ma, G. Lu, J. Catal. 353 (2017) 162–170.
[50] K. Maeda, K. Domen, J. Phys. Chem. C 111 (2007) 7851–7861.
[51] Q. Li, B. Guo, J. Yu, J. Ran, B. Zhang, H. Yan, J.R. Gong, J. Am. Chem. Soc. 133 (2011) 10878–10884.
[52] A. Iwase, Y.H. Ng, Y. Ishiguro, A. Kudo, R. Amal, J. Am. Chem. Soc. 133 (2011) 11054–11057.
[53] Q. Wang, T. Hisatomi, Q. Jia, H. Tokudome, M. Zhong, C. Wang, Z. Pan, T. Takata, M. Nakabayashi, N. Shibata, Y. Li, I.D. Sharp, A. Kudo, T. Yamada, K. Domen, Nat. Mater. 15 (2016) 611–615.
[54] Q. Li, H. Meng, P. Zhou, Y. Zheng, J. Wang, J. Yu, J. Gong, ACS Catal. 3 (2013) 882–889.
[55] H.N. Kim, T.W. Kim, I.Y. Kim, S.J. Hwang, Adv. Funct. Mater. 21 (2011) 3111–3118.
[56] Y.H. Li, J. Xing, Z.J. Chen, Z. Li, F. Tian, L.R. Zheng, H.F. Wang, P. Hu, H.J. Zhao, H.G. Yang, Nat. Commun. 4 (2013) 2500.
[57] D. Wang, A. Pierre, M.G. Kibria, K. Cui, X. Han, K.H. Bevan, H. Guo, S. Paradis, A.R. Hakima, Z. Mi, Nano Lett. 11 (2011) 2353–2357.
[58] T.F. Berto, K.E. Sanwald, J.P. Byers, N.D. Browning, O.Y. Gutierrez, J.A. Lercher, J. Phys. Chem. Lett. 7 (2016) 4358–4362.
[59] R. Abe, K. Sayama, H. Arakawa, Chem. Phys. Lett. 371 (2003) 360–364.
[60] A.V. Bakulin, S.E. Kulkova, S.V. Eremeev, O.E. Tereshchenko, J. Phys. Chem. C 118 (2014) 10097–10105.
[61] A. Panchenko, M.T.M. Koper, T.E. Shubina, S.J. Mitchell, E. Roduner, J. Electrochem. Soc. 151 (2004) A2016–A2027.
[62] W. Zhen, H. Gao, B. Tian, J. Ma, G. Lu, A.C.S. Appl, Mater. Inter. 8 (2016) 10808–10819.
[63] B. Wang, L. Song, R. Zhang, Appl. Surf. Sci. 258 (2012) 3714–3722.
[64] B. Tian, Z. Li, W. Zhen, G. Lu, J. Phys. Chem. C 120 (2016) 6409–6415.
[65] X. Lin, J. Lu, J. Liu, Y. Tang, H. Zhu, Chem. Phys. 483–484 (2017) 156–164.
[66] J.F. Guayaquil-Sosa, B. Serrano-Rosales, P.J. Valadés-Pelayo, H. de Lasa, Appl. Catal. B 211 (2017) 337–348.
[67] P. Wang, S. Zhan, Y. Xia, S. Ma, Q. Zhou, Y. Li, Appl. Catal. B 207 (2017) 335–346.
[68] Y. Li, C. Zhang, J. Ma, M. Chen, H. Deng, H. He, Appl. Catal. B 217 (2017) 560–569.
[69] X. Zhu, B. Cheng, J. Yu, W. Ho, Appl. Surf. Sci. 364 (2016) 808–814.
[70] Z. Wang, W. Wu, Q. Xu, G. Li, S. Liu, X. Jia, Y. Qin, Z.L. Wang, Nano Energy 38 (2017) 518–525.
[71] L. Nie, P. Zhou, J. Yu, M. Jaroniec, J. Mol. Catal. A. 390 (2014) 7–13.
[72] M. Zhang, C. Shao, Z. Guo, Z. Zhang, J. Mu, T. Cao, Y. Liu, A.C.S. Appl, Mater. Inter. 3 (2011) 369–377.
[73] C. Wang, C. Shao, X. Zhang, Y. Liu, Inorg. Chem. 48 (2009) 7261–7268.
[74] J. Jin, C. Wang, X. Ren, S. Huang, M. Wu, L. Chen, T. Hasan, B. Wang, Y. Li, B.L. Su, Nano Energy 38 (2017) 118–126.
[75] Z. Zhang, Z. Wang, S.W. Cao, C. Xue, J. Phys. Chem. C 117 (2013) 25939–25947.
[76] Y. Si, S. Cao, Z. Wu, Y. Ji, Y. Mi, X. Wu, X. Liu, L. Piao, Nano Energy 41 (2017) 488–493.
[77] J.G. Yu, W.G. Wang, B. Cheng, B.L. Su, J. Phys. Chem. C 113 (2009) 6743–6750.
[78] S. Weon, J. Kim, W. Choi, Appl. Catal. B 220 (2018) 1–8.
[79] Q. Wang, C.C. Chen, D. Zhao, W.H. Ma, J.C. Zhao, Langmuir 24 (2008) 7338–7345.
[80] S. Ponnaiah, P. Periakaruppan, B. Vellaichamy, B. Nagulan, J. Colloid Interf. Sci. 512 (2018) 219–230.
[81] Y. Guo, J. Zhao, H. Zhang, S. Yang, J. Qi, Z. Wang, H. Xu, Dyes Pigm. 66 (2005) 123–128.
[82] Y. Cho, H. Kim, S. Lee, W. Choi, J. Catal. 330 (2015) 387–395.
[83] Z. He, M. Hu, X. Wang, Catal. Today 302 (2018) 136–145.
[84] Z. Duan, G. Wang, J. Phys. Chem. C 117 (2013) 6284–6292.
[85] G. Pacchioni, Electrochim. Acta 41 (1996) 2285–2291.